

The Importance of Accurate Boundary Condition in Obtaining Reliable Shearing Stresses on a Torsional Finite Element Simulation

Jairo Aparecido Martins
Research & Development
DESCH North America
Cambridge, Ontario, Canada
Jairo.martins@desch.com

Estaner Claro Romão
Department of Environmental Engineering
Lorena School of Engineering, University of São Paulo
Lorena, São Paulo, Brasil
estaner23@usp.br

Received: 21 December 2021 | Accepted: 3 January 2022

Abstract- Many combustion engines and electric motors drive machines or equipment by turning a shaft and thus producing work. As a relevant part of a machine principle, torque transference deserves deep analysis regarding the techniques that determine precisely the Finite Element (FE) boundary conditions that are to be applied. This work presents a shaft loaded with a torque that causes torsion and results in shear stresses in the shaft material. In this context, when designing and calculating a shaft to transfer torque, virtual analysis like FE Analysis (FEA) must replicate the reality as accurately as possible. Indeed, slight changes in load and constraint in a virtual simulation can produce considerably different shear stresses and unrealistic results. This paper aims to demonstrate how distinct boundary conditions for the same torque transference can result in very different results when a simulation does not comply with reality. The results showed the importance of being very attentive when applying loads and constraints on a shaft under torsion while calculating it via FEA.

Keywords- torsion; numerical simulation; boundary conditions

I. INTRODUCTION

Finite Element Analysis (FEA) is becoming increasingly popular among design engineers who use it as a product-design tool. Being safe and cost-efficient, the use of FEA as a product-design tool requires training, practice, and, mainly, experience, which is not present in the undergraduate curricula of mechanical engineering programs due to time constraints [1-4]. Among applications and calculations by the tool, there are many books on metallurgy and mechanics that describe many types of loads and boundary conditions to consider, torque being one among them as an important load.

Authors in [5-7] presented solid concepts and provided examples of real applications for readers. In addition, there are scientific works that calculate and analyze torque for several interesting applications. Authors in [8] developed a FEA program based on FORTRAN for analyzing working behavior and calculating torque and drag during oil extraction. The values of displacement obtained from the FEA model matched those from the analytical model. Authors in [9] presented

different methods for the calculation of torque as a function of rotation angle in an electrical machine. The results obtained by the distinct methodology were compared with the experimental data, which allowed attaining practical information concerning the advantages and limitations of each method. Authors in [10] investigated techniques for the optimal design of permanent magnet motors considering rotation. By applying the optimal design method, the authors reduced about 40% of the volume of the permanent magnet of the IPM motor and about 15% of the torque ripple. This reinforced the idea that most of the FE models should also be evaluated experimentally in order to be calibrated with reality. However, even in a virtual simulation platform, the model has to be as much realistic as possible and should utilize the most accurate and realistic boundary techniques. In this context, authors in [11] studied the simplification of the design geometry in the FEA of structural and other continuum problems and concluded that strategies for identifying possible idealizations, controlling their application, and estimating the associated errors appear to be feasible. In particular, authors in [12] assessed the mechanical properties of glass/metal joints. In his study, a Finite Element Method (FEM) was implemented to analyze the torsional shear strength test designed for glass-ceramic/steel joints aiming towards solid oxide fuel/electrolysis cell application. The authors concluded that the difference between the analytically derived nominal shear strength, and the real critical shear stress derived via simulation, reduces with decreasing fracture torque.

The boundary condition results might end up differently and some of them wrong if the simulation is not as close to reality as it could be. To the best of our knowledge, there are no papers that describe the impacts on the results on FE simulations when torque incurs on different (non-realistic) boundary conditions. Many pieces of literature and videos on media teach watchers how to run a FE simulation. However, not always the presentations are correct and precise. For instance, [13-15] described a few boundaries conditions for torque application incompatible with reality and can cause problems in the field. For this reason, this paper aims to demonstrate how distinct boundary conditions for the same

Corresponding author: Estaner Claro Romão

torque transference can result in expressively distinct results when a simulation does not comply with reality.

II. MATERIAL AND METHODS

This study used classical equations to determine the torque to utilize in the FEM as a torsion load. The shaft used on the simulations had one extreme constrained and another one receiving a torsional momentum (torque). To calculate the shearing stresses by numerical simulation, the shaft diameter was kept fixed at 10mm, and the length changed throughout the simulations. In addition, the loading region, where torque incurred, was altered in the simulations, from face to partial body, to whole body, and finally using an arm like if it were a wrench. Two opposing torques (T) produce a twisting load along the axis of a circular shaft, resulting in a total shear stress distribution (τ) given by (1) [16]:

$$\tau = \frac{T \cdot r}{J} \quad (1)$$

where $0 \leq r \leq R$. r is the distance from the center of the shaft and R is the outside radius, both in mm. Since the diameter of the shaft is fixed, therefore $R \cdot T$ is the applied torque (N.mm), τ the shear stress (MPa), and J is the moment of polar inertia (mm^4), which is given by (2):

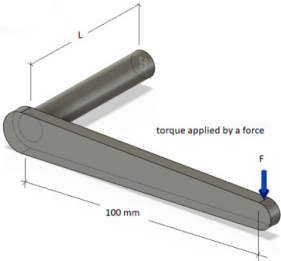
$$J = \frac{1}{2} \cdot \pi \cdot R^4 \quad (2)$$

Therefore combining (1) to (2) results to:

$$\tau = \frac{2 \cdot T}{\pi \cdot R^3} \text{ or } T = \frac{\tau \cdot \pi \cdot R^3}{2} \quad (3)$$

Assuming a fixed shearing stress of 100MPa as well as a fixed shaft diameter of 10mm, the torque result comes from (3) and is fixed at 19,635N.mm. It is relevant to highlight that since the purpose of the simulation is to apply 19,635N.mm as a total torque, only half of the torque was input on the shaft because the torque reaction generates the whole aimed torque. The fixed torque value was used throughout all simulations when running the FEA. In addition, each simulation had the shaft length altered progressively from 10mm to 1,000mm. For numerical simulations Autodesk F360 was utilized, considering a linear-elastic analysis and as an output the von Mises stress [18-20]. As seen in Table I, the same torque was input in four different ways. On the shaft face, along the shaft body, at a particular region, and by applying a vertical force on the arm attached to the shaft. In terms of mesh configuration, the same mesh for all simulations was utilized, which followed a maximum number of mesh refinement of 6, a convergence tolerance of 5%, a portion (40%) of elements to refine it, and an average element size of 10%.

TABLE I. BOUNDARY CONDITIONS FOR A SHAFT DIAMETER 10mm LOADED WITH A FIXED TORQUE OF 9,817.5N.mm.

Simulation boundaries	Description
	Shaft 10mm in diameter with length from 10 to 1,000mm. Simulation with constraint at back surface and torque applied on shaft face (SF).
	Shaft 10mm in diameter with length from 10 to 1,000mm. Simulation with constraint at the back surface and torque applied on shaft whole body (SWB).
	Shaft 10mm in diameter with length from 10 to 1,000mm. Simulation with constraint at the back surface and a torque applied on a body region of 15mm length (1.5 times the shaft diameter) (SPB).
	Shaft 10mm in diameter with length from 10 to 1,000mm. Simulation with constraint at the back surface and force applied on a wrench extreme (SWR).

III. RESULTS AND DISCUSSION

Figures 1 to 4 show the different equivalent stress (von Mises) in MPa for the following configurations: shaft with a torque applied at its face (SF), shaft torque body (SWB), shaft region (slip body) torque (SPB), and force with arm like a wrench (SWR). Figure 1 shows the maximum stress at the edge of the face where the torque is transmitted, and it reaches 105.1MPa for a shaft length of 60mm (SF). Figure 2 shows a von Mises stress of 89.08MPa at constraint face.



Fig. 1. Example of a shaft (10mm diameter × 60mm) simulated with a torque applied on the face (SF).

SWB differed from the SF condition, from 105.1MPa to 89.08MPa. Not only the shear stress intensity was different, but also the stress localization. Unlike SF, the maximum torque for SWB moved to the opposite side from the torque load. Figure 3 shows a change in torque from SWB to SPB. At this case, the maximum shearing stress was seen where the load was applied, and it reached 92.79MPa. When an arm was added (SWR), then a force was applied to simulate the torque. The shearing stress reached 107.5MPa and was positioned close to the shaft constraint (Figure 4). Figure 5 shows the variance of shearing stress for 10mm shaft diameter with a length changing from 10mm to 1,000mm, and affixed torque of 9,817.5N.mm applied on the shaft face (SF). For a short shaft (10mm length), the stress was significantly higher than the calculated value of 100MPa, reaching a peak of 180MPa. The diameter and length for this condition are the same and fixed at 10mm. There is a wide stress variance and up and down change for lengths from 10 to 200mm when the stress decreases and reaches a value close to the calculated value. However, after 200mm, the measured stress is unstable and has a high standard deviation as seen in Table II and Figures 9 and 10.

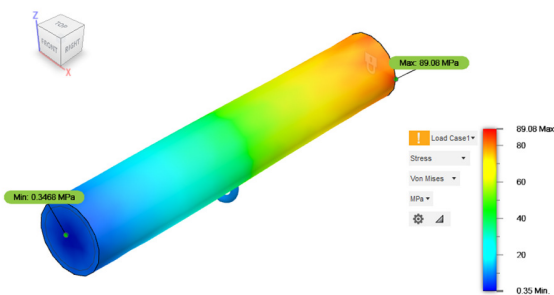


Fig. 2. Example of a shaft (10mm diameter × 60mm) simulated with a torque applied on the body (SWB).

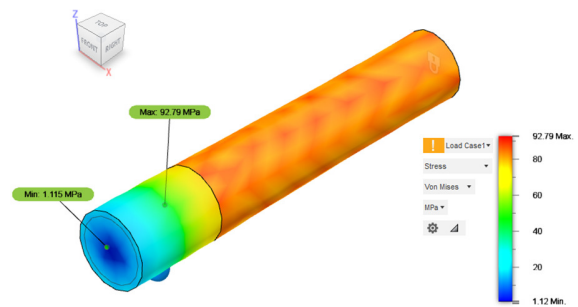


Fig. 3. Example of a shaft (10mm diameter × 60mm) simulated with a torque applied on a region of the body (SPB).

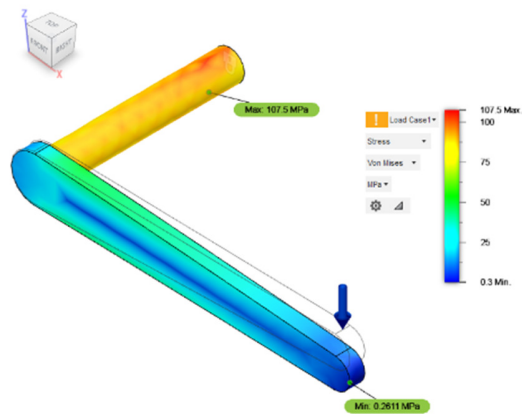


Fig. 4. Example of a shaft (10mm diameter × 60mm) simulated with a force applied on arm (SWR).

Moreover, the standard deviation changes, depending on the length. It begins from 28MPa for lengths between 10mm and 100mm and reduces to 14MPa for lengths between 100mm and 300mm and it ends up with 12MPa from lengths between 300mm and 1,000mm.

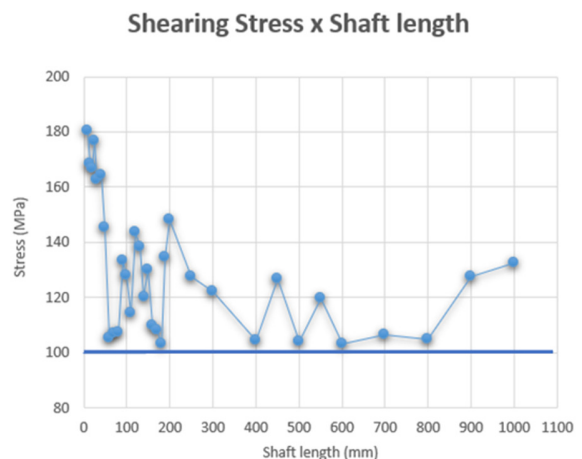


Fig. 5. Shear stress with a torque applied on shaft face versus different lengths (SF).

When stress is applied to the shaft body (SWB), it reaches the highest stress level of 102MPa to a length of 10mm (Figure

6), thereafter it drops with length increment, reaching 86MPa when the length is 30mm. Soon after this point, the stress starts increasing again and it reaches 95MPa for a length maximum of 1,000mm. The standard deviation changes from 4MPa for lengths between 10mm and 100mm, then it reduces to 1MPa for lengths between 100mm and 300mm and ends up at 1MPa for lengths between 300mm and 1,000mm.

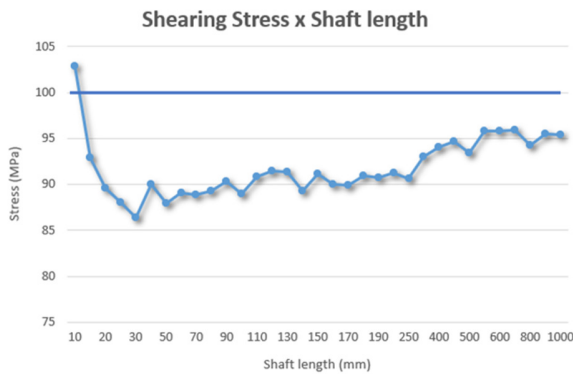


Fig. 6. Shear stress with a torque applied on shaft body versus different lengths (SWB).

When the torque is loaded on a specific and limited region of the shaft (SPB), the stress starts with a high value for a short shaft (103MPa for 10mm length), then it drops to 93MPa, thereon stresses fluctuate up and down and reach 95MPa at 1,000mm length (Figure 7). When it comes to standard deviation, it changes from 3MPa for lengths between 10mm and 100mm, then it reduces to 1MPa for lengths between 100mm and 300mm, and ends up at 1MPa for lengths between 300mm and 1,000mm. This presents a quite similar standard deviation when compared with the previous condition (SWB).

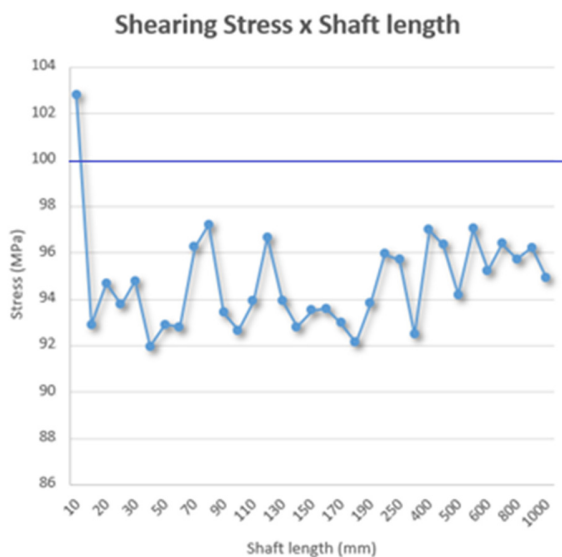


Fig. 7. Shear stress with a torque applied on shaft specific region versus different length (SPB).

A distinct behavior from previous situations is verified for a shaft that has an arm with a force-generating a torque (SWR) as shown in Figure 8. The shearing stress is pretty close to 100MPa as previously calculated analytically, but for 120mm and onwards it raises continually and moderately until 300mm when there is a steep inclination on the graph, demonstrating a mechanical instability. The standard deviation changes from 2MPa for lengths between 10mm and 100mm, then it goes up to 15MPa for lengths between 100mm and 300mm and it steeped up considerably to 89MPa for lengths between 300mm and 1,000mm. This presents the highest instability of all previous conditions. This stability comes from a lack of rigidity of the bar when it gets longer and longer until a point where the combination becomes totally mechanically unstable (uneven).

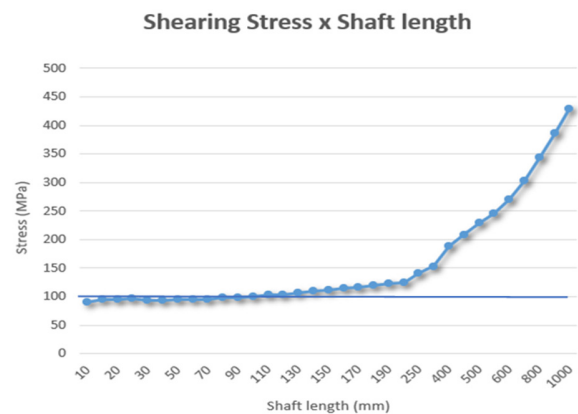


Fig. 8. Shear stress with a torque applied on shaft by a force applied on an arm (SWR).

Table II shows the partial calculations of shearing stress averages and standard deviations. It compiles variations of von Mises stress average and how data deviation occurs based on standard deviation. The shaft with a torque applied on a specific region showed the closer value to the calculated 100MPa (95MPa) and the lower standard deviation throughout all shaft lengths. In Figures 9 and 10, there is a comparison among stresses generated by torques applied on a region of a shaft body. A line at 100MPa is traced to help compare FEA to the analytical calculated value. The condition where the torque is applied on the face of the bar (Figure 9 left) shows that for short bars, the von Mises stress is higher, then it decreases constantly until the length of 1,000mm, which is 100 times the diameter of the shaft.

Therefore, this condition shows stress values that, when compared with the analytical calculation, do not seem accurate enough or reliable. When the torque is applied on the whole body (Figure 9(b)), the von Mises values are similar, and close to 90MPa for the full range of lengths with a standard value very low for short shafts as well as for longer bars. This means that the stress value is only 10% lower than the analytical calculated von Mises stress. When the torque is applied on a specific region of the bar, established as 1.5 times the shaft diameter (Figure 10(a)), the stress values were very close to the analytical calculation and varied from 95 to 96MPa.

TABLE II. DISTINCT VALUES FOR EACH CONFIGURATION

Condition	Von Mises stress (MPa) Average $10 \leq L \leq 100$	Calculated stress (τ) (MPa) StDev $10 \leq L \leq 100$	Von Mises stress (MPa) Average $100 \leq L \leq 300$	Calculated stress (τ) (MPa) StDev $100 \leq L \leq 300$	Von Mises (MPa) Average $300 \leq L \leq 1,000$	Calculated stress (τ) (MPa) StDev $300 \leq L \leq 1,000$
SF	145	28	125	14	115	12
SWB	90	4	91	1	95	1
SPB	95	3	94	1	96	1
SWR	95	2	117	15	276	89

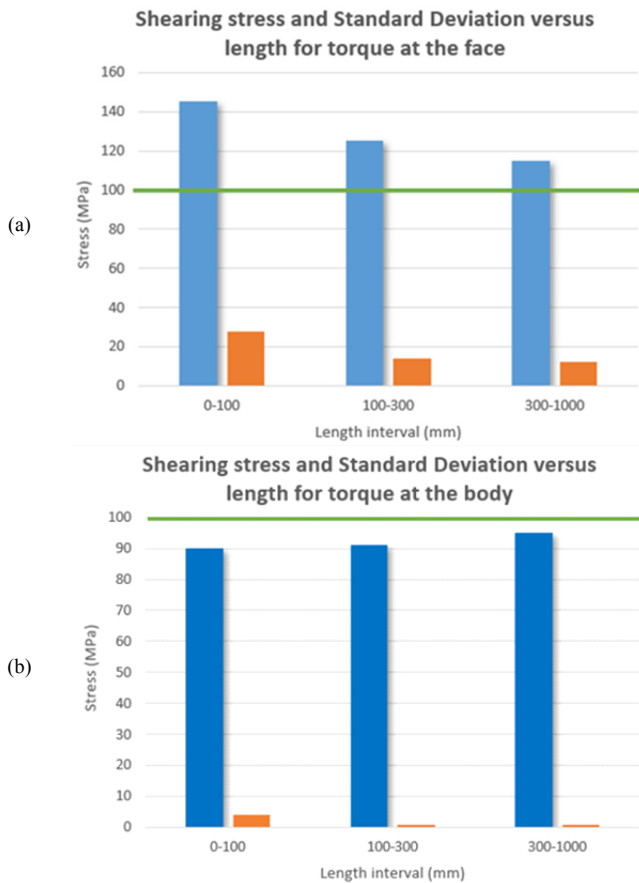


Fig. 9. (a) Torques and standard deviation from distinct length intervals for (a) SF, (b) SWB.

This configuration represents remarkably real conditions seen on machines and equipment where an electrical motor has a coupling assembled on a specific length of the shaft. The final configuration applied a torque indirectly on the shaft by using an arm. At the extreme of the arm, the force that generates the torque was applied. At this case, the value was very close to the analytical one (100MPa analytical value versus 95MPa for simulation) for short shafts smaller than 100mm. For shafts with lengths between 100mm and 300mm the value surpassed the analytical value (117MPa versus 100MPa) and reached 276MPa, which is completely unrealistic.

The configurations were ranked comparatively with the analytical calculation. The closer value was verified at the SWR condition, to shaft length from 10 to 100mm, presenting a shear stress average of 95MPa and a standard deviation of

2MPa. The second was the SPB condition, with also 95MPa for shear stress and a standard deviation of 3MPa. The third condition was SWB, with an average of 90MPa and a standard deviation of 4MPa, and the last one was SF with an average of 145MPa and standard deviation of 28MPa, see Table II and Figures 9 and 10.

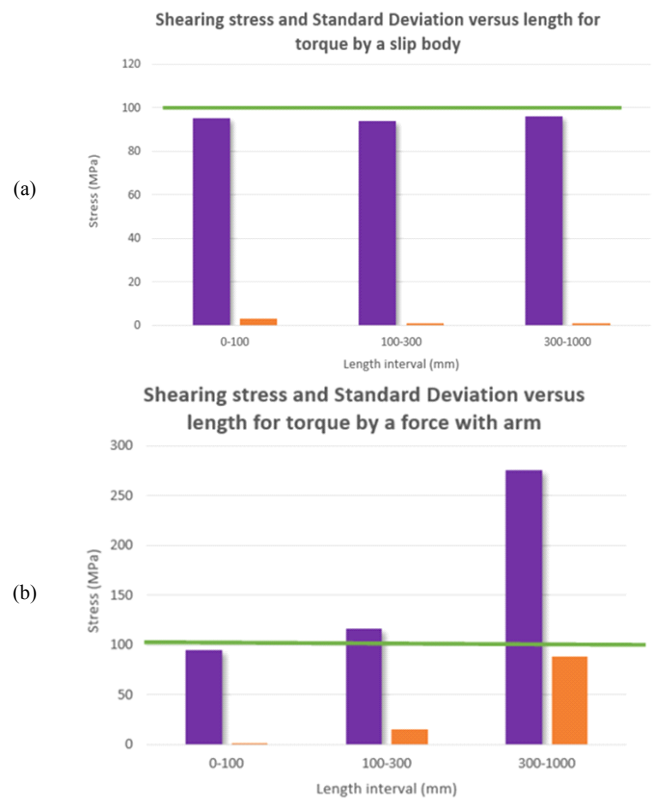


Fig. 10. Torques and standard deviation from distinct length intervals for (a) torque applied on a specific region of the shaft (SPB), (b) torque inputted on an arm like a wrench (SWR).

For shaft's lengths from 100 to 300mm, the sequence changed. The SPB condition ranked first with a von Mises Stress of 94MPa and standard deviation of 1MPa, the second was SWB with a von Mises Stress of 91MPa and standard deviation of 1MPa. SWR was the third with a von Mises Stress of 117MPa and standard deviation of 15MPa, and SF was last exhibiting a von Mises Stress of 125MPa and standard deviation of 14MPa. For longer positions (300 to 1,000mm) there was another change in positions. First was SPB with a von Mises Stress of 96MPa and standard deviation of 1MPa, then

SWB with a von Mises Stress of 95MPa and standard deviation of 1MPa. The third was SF with a von Mises Stress of 115MPa and standard deviation of 12MPa, and SWR was last with a von Mises stress of 276MPa and standard deviation of 89MPa.

IV. CONCLUSIONS

This paper aimed to demonstrate how distinct boundary conditions for the same torque transference could result in different results when a simulation does not comply with reality. The results showed that unrealistic boundary conditions might result in unlikely shearing stresses and depending on the precision aimed, the results can lead to wrong conclusions, sometimes leading to failures. The results reinforced that realistic simulations are compulsory when working with FEA, even for a simple load as torsion. For this simulation in particular, the calculation of shearing stresses' averages and standard deviation within intervals helped to define the most appropriate way to apply a torque on a shaft with the presented dimensions. This simplification can lead to wrong conclusions on a system design and generate failure. Therefore, close attention and comparison between the simulation and reality are essential in order to produce a successful project.

To sum up, many machines and equipment have alternate ways of transferring movement by torsion. It can be by a coupling to transfer torque from an electrical motor to a system or a mechanism lever to produce a parallel actuating system. However, the real matter is that the FEA system can provide precise outputs only with precise and realistic inputs (boundary conditions).

ACKNOWLEDGMENT

The authors acknowledge the financial support by CAPES (process number 23038.000263/2022-19).

REFERENCES

- [1] P. M. Kurowski, "Teaching Finite Element Analysis For Design Engineers," in *Canadian Design Engineering Network Conference*, Toronto, Canada, Jul. 2006, pp. 203–234, <https://doi.org/10.24908/pceea.v0i0.3839>.
- [2] P. M. Kurowski, *Finite Element Analysis For Design Engineers*. Warrendale, PA, USA: SAE International, 2004.
- [3] P. Kurowski, "Chapter 3: Fundamental Concepts of Finite Element Analysis," in *Finite Element Analysis for Design Engineers*, Warrendale, PA, USA: SAE International, 2017, pp. 17–33.
- [4] I. Widiastuti and C. W. Budiyo, "Applying an Experiential Learning Cycle with the Aid of Finite Element Analysis in Engineering Education," *Journal of Turkish Science Education*, vol. 15, no. Special, pp. 97–103, Dec. 2018.
- [5] G. Dieter, *Mechanical Metallurgy*. New York, NY, USA: McGraw Hill, 1968.
- [6] T. Brown, *Mark's Calculations For Machine Design*. New York, NY, USA: McGraw-Hill, 2005.
- [7] G. E. O. Giacaglia, *Mecanica Geral*. Chicago, IL, USA: Campus, 1982.
- [8] A. Wu, G. Hareland, and M. Fazelzadeh, "Torque & Drag Analysis Using Finite Element Method," *Modern Applied Science*, vol. 5, no. 6, pp. 13–27, Nov. 2011, <https://doi.org/10.5539/mas.v5n6p13>.
- [9] N. Sadowski, Y. Lefevre, M. Lajoie-Mazenc, and J. Cros, "Finite element torque calculation in electrical machines while considering the movement," *IEEE Transactions on Magnetics*, vol. 28, no. 2, pp. 1410–1413, Mar. 1992, <https://doi.org/10.1109/20.123957>.
- [10] T. Ohnishi and N. Takahashi, "Optimal design of efficient IPM motor using finite element method," *IEEE Transactions on Magnetics*, vol. 36, no. 5, pp. 3537–3539, Sep. 2000, <https://doi.org/10.1109/20.908891>.
- [11] C. G. Armstrong, "Modelling requirements for finite-element analysis," *Computer-Aided Design*, vol. 26, no. 7, pp. 573–578, Jul. 1994, [https://doi.org/10.1016/0010-4485\(94\)90088-4](https://doi.org/10.1016/0010-4485(94)90088-4).
- [12] M. Fakouri Hasanabadi, J. Malzbender, S. M. Groß-Barsnick, H. Abdoli, A. H. Kokabi, and M. A. Faghihi-Sani, "Finite element optimization of sample geometry for measuring the torsional shear strength of glass/metal joints," *Ceramics International*, vol. 46, no. 4, pp. 4857–4863, Mar. 2020, <https://doi.org/10.1016/j.ceramint.2019.10.221>.
- [13] L. Zhixin, L. Xiaoqing, C. Xuedong, and C. Lumin, "The Study on Boundary Conditions to the Effect of Mode Analysis in FEA," *China Mechanical Engineering*, vol. 19, no. 9, pp. 0–1054, May 2008.
- [14] P. Bratley, B. L. Fox, and L. E. Schrage, *A Guide to Simulation*. New York, NY, USA: Springer, 1987.
- [15] R. G. Ingalls, "Introduction to simulation," in *Winter Simulation Conference*, Phoenix, AZ, USA, Dec. 2011, pp. 1374–1388, <https://doi.org/10.1109/WSC.2011.6147858>.
- [16] T. Brown, *Mark's Calculations For Machine Design*, 1st edition. New York, NY, USA: McGraw Hill, 2005.
- [17] "Learn Fusion 360 | Fusion 360 Support, Tutorials & Videos." <https://www.autodesk.ca/en/products/fusion-360/learn-support> (accessed Mar. 17, 2022).
- [18] M. M. Teymoori and J. M. Ahangarkolaei, "A Tunable Capacitor Based on MEMS Technology for RF Applications," *Engineering, Technology & Applied Science Research*, vol. 6, no. 3, pp. 982–986, Jun. 2016, <https://doi.org/10.48084/etasr.679>.
- [19] S. Bekkouche and M. Kadja, "Numerical Analysis of Density-Driven Reactive Flows in Hele-Shaw Cell Geometry," *Engineering, Technology & Applied Science Research*, vol. 10, no. 2, pp. 5434–5440, Apr. 2020, <https://doi.org/10.48084/etasr.3349>.
- [20] E. C. Romao and L. H. P. de Assis, "Numerical Simulation of 1D Unsteady Heat Conduction-Convection in Spherical and Cylindrical Coordinates by Fourth-Order FDM," *Engineering, Technology & Applied Science Research*, vol. 8, no. 1, pp. 2389–2392, Feb. 2018, <https://doi.org/10.48084/etasr.1724>.